The EMBO Journal Vol.17 No.21 pp.6155–6167, 1998

Periplasmic chaperone recognition motif of subunits mediates quaternary interactions in the pilus

Gabriel E.Soto, Karen W.Dodson, Derek Ogg[1], Christopher Liu, John Heuser[2], Stefan Knight[3], Jan Kihlberg[4], C.Hal Jones[5] and Scott J.Hultgren[6]

Department of Molecular Microbiology and [2]Department of Cell Biology and Physiology, Washington University School of Medicine, St Louis, MO 63110, USA, [1]Structural Chemistry N62.6, Pharmacia and Upjohn, 112 87 Stockholm, [3]Swedish University of Agricultural Sciences, Uppsala Biomedical Centre, Department of Molecular Biology, P.O. Box 590, S-751 24 Uppsala, [4]Department of Organic Chemistry, Umeå University, S-901 87 Umeå, Sweden and [5]SIGA Pharmaceuticals, Inc., Research and Development Division, 4575 SW Research Way, Suite 230, Corvallis, OR 97333, USA

[6]Corresponding author

The class of proteins collectively known as periplasmic immunoglobulin-like chaperones play an essential role in the assembly of a diverse set of adhesive organelles used by pathogenic strains of Gram-negative bacteria. Herein, we present a combination of genetic and structural data that sheds new light on chaperone–subunit and subunit–subunit interactions in the prototypical P pilus system, and provides new insights into how PapD controls pilus biogenesis. New crystallographic data of PapD with the C-terminal fragment of a subunit suggest a mechanism for how periplasmic chaperones mediate the extraction of pilus subunits from the inner membrane, a prerequisite step for subunit folding. In addition, the conserved N- and C-terminal regions of pilus subunits are shown to participate in the quaternary interactions of the mature pilus following their uncapping by the chaperone. By coupling the folding of subunit proteins to the capping of their nascent assembly surfaces, periplasmic chaperones are thereby able to protect pilus subunits from premature oligomerization until their delivery to the outer membrane assembly site.

Keywords: bacterial fimbriae/macromolecular systems/molecular chaperones/protein folding/X-ray crystallography

Introduction

The assembly of bacterial pili represents one of the best-characterized model systems available for the study of macromolecular assembly. These adhesive organelles play a crucial role in the pathogenesis of many virulent bacterial strains, as they mediate binding between the invading organisms and complementary receptors on the surfaces of host cells (Hultgren *et al.*, 1996). Their assembly requires the ordered progression of multiple protein–protein recognition events, which in many cases are orchestrated by the ubiquitous chaperone–usher pathway. This pathway is involved in the assembly of >25 of these and other non-pilus organelles of attachment, and its study has provided insight into the basic biological processes of chaperone-assisted import, folding and targeting of proteins to specific assembly sites (Hung *et al.*, 1996). The key features of this pathway are well illustrated by the prototypical P pili. These organelles are expressed in up to 90% of uropathogenic strains of *Escherichia coli* isolated from patients with pyelonephritis, versus only 5–10% of human fecal *E.coli* isolates (Hultgren *et al.*, 1996).

Encoded by genes of the *pap* operon, P pili are oligomeric structures containing a distal tip fibrillum attached to a pilus rod (Kuehn *et al.*, 1992). The tip fibrillum is comprised of repeating PapE subunits and contains the PapG adhesin at its distal end, which is thought to be connected to the tip via the PapF adaptor protein (Jacob-Dubuisson *et al.*, 1993). The pilus rod is made up exclusively of PapA subunits arranged in a right-handed helical cylinder and is thought to be connected to the tip fibrillum via the PapK adaptor (Jacob-Dubuisson *et al.*, 1993). PapH appears to terminate pilus assembly and is important for the proper anchoring of the rod to the bacterial cell's outer membrane (Baga *et al.*, 1987). Pilus assembly *in vivo* also requires the expression of two additional proteins encoded by the *pap* operon: the periplasmic chaperone PapD and the outer membrane usher PapC. The latter forms an oligomeric pore (Thanassi *et al.*, 1998) in the outer membrane that regulates pilus assembly at least in part through kinetic partitioning of the chaperone–subunit pre-assembly complexes, with preferential binding of the chaperone–adhesin complex serving to initiate pilus assembly (Dodson *et al.*, 1993; Saulino *et al.*, 1998).

PapD is the prototypical member of a highly conserved family of chaperones that are required for the assembly of both pilus and non-pilus adhesive organelles (Holmgren *et al.*, 1992; Hung *et al.*, 1996). PapD is known to play a multifunctional role in pilus assembly: (i) it mediates the partitioning of nascently translocated subunits out of the inner cytoplasmic membrane and into the periplasm; (ii) it is involved in the folding of nascent subunits into a native-like conformation; and (iii) it prevents the premature aggregation of subunits within the periplasmic space, which is otherwise toxic to the bacterial cell (Jones *et al.*, 1997). However, the lack of any data at atomic level resolution on the structure of these hetero-oligomeric organelles or of a complete chaperone–subunit complex, together with the inability to obtain stable subunits in the absence of chaperone, has impeded attempts to determine precisely how chaperones carry out these functions *in vivo*.

At present, it is known that periplasmic chaperones like PapD form complexes with pilus subunits prior to their assembly. Several lines of evidence strongly indicate that

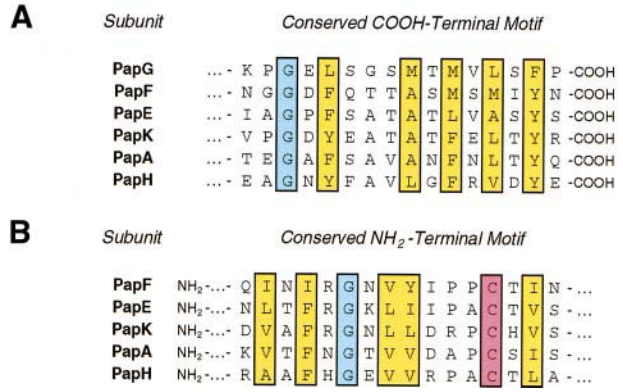

Fig. 1. (**A**) Conserved C-terminal motif present in pilus subunits assembled by the PapD chaperone. For a comprehensive alignment of this region among all adhesive organelle subunits known to be assembled by members of the immunoglobulin-like chaperone superfamily, see Hung *et al*. (1996). Key: yellow boxed residues, conserved alternating hydrophobic residues; blue boxed residues, conserved glycine at position 14 from the C-terminus. (**B**) Conserved N-terminal motif present in pilus subunits assembled by the PapD chaperone. Key: yellow boxed residues, conserved alternating hydrophobic residues; blue boxed residues, conserved glycine; pink boxed residues, conserved cysteine.

chaperones recognize and bind to a highly conserved C-terminal motif present in all pilus subunits assembled by PapD-like chaperones (Figure 1A). This motif is characterized by a series of alternating hydrophobic residues flanked by a glycine located 14 residues upstream from the C-terminus and a penultimate tyrosine. The evidence that chaperones bind to this region includes: (i) the finding that deletion of this C-terminal region abolishes chaperone–subunit complex formation (Hultgren *et al.*, 1989); (ii) the demonstration that PapD specifically binds synthetic peptides whose sequences correspond to the C-terminal region of P pilus subunits; and (iii) the co-crystallization of PapD bound to a peptide corresponding to the last 19 amino acids of the PapG adhesin (Kuehn *et al.*, 1993).

In this study, we elucidated the molecular basis by which periplasmic chaperones orchestrate the assembly of these hetero-oligomeric organelles. In a series of complementary experiments, we characterized the structural aspects of chaperone–subunit recognition in the pre-assembly complexes and subunit–subunit interactions in the assembled pilus structure. The data argue for a model in which the conserved chaperone-binding motifs of subunits are mapped to one or more assembly surfaces that participate in quaternary subunit–subunit interactions after chaperone uncapping. Furthermore, the formation of these assembly surfaces may be coupled to their capping and subsequent protection from premature assembly following chaperone-mediated extraction of the subunits from the inner membrane.

Results

Effect of C-terminal mutations on the stability of PapG–PapF and PapG–PapD complexes

In order to investigate the possibility that the conserved C-terminal motif of pilus subunits is involved in mediating subunit–subunit contacts, we used site-directed mutagenesis to modify the pattern of alternating hydrophobic

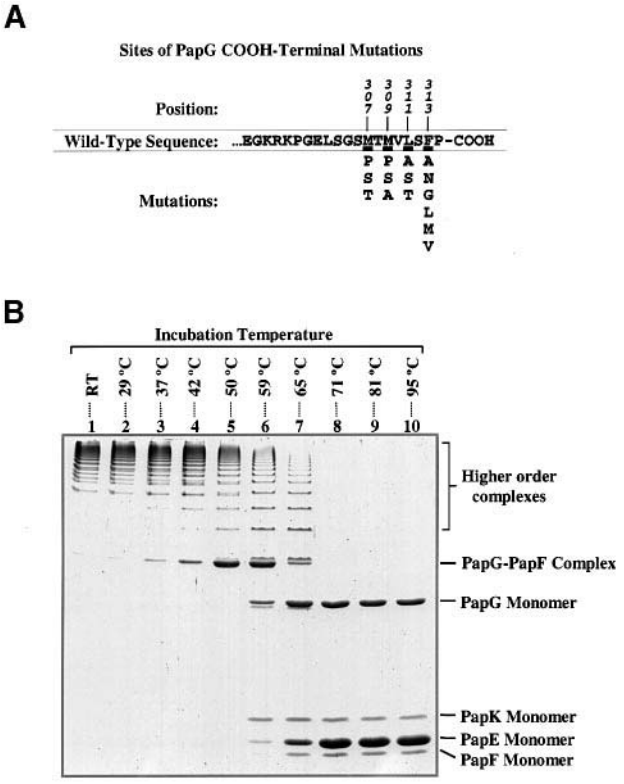

Fig. 2. (**A**) Sequence of the C-terminal region of the PapG adhesin and summary of site-directed mutants used to examine PapG–PapF interactions. Underlined positions are conserved across other pilus subunits. (**B**) Tip fibrillae containing either wild-type PapG or one of 15 point mutants were prepared and incubated in SDS loading buffer for 10 min at incremental temperatures prior to analysis by SDS–PAGE. Shown here are the data for tips isolated from cells expressing wild-type PapG. As seen in this Coomassie Blue-stained gel, bands corresponding to PapG–PapF complexes and higher order PapK–$(PapE)_n$–PapF–PapG assemblies were observed at incubation temperatures up to 65°C. At 71°C and above; however, the PapG–PapF and higher order complexes were completely dissociated, releasing PapG as a clearly resolved monomer. The identity of the PapG band was confirmed by immunoblotting with α-PapG-specific antisera. The identity of the PapF–PapG band was confirmed by its excision from a duplicate gel and subsequent analysis by SDS–PAGE and immunoblotting with α-tip antisera following incubation at 95°C.

residues at positions 307, 309, 311 and 313 of the PapG adhesin (corresponding to positions 8′, 6′, 4′ and 2′, respectively, counting from the C-terminus of the protein). We examined the effects of 15 distinct point mutations within this region with respect to PapG–PapF interactions in the mature pilus, as measured by the relative temperature required for dissociation of PapG from PapF in purified pilus tips (Figure 2). The results of these experiments are summarized in Table I. Generally speaking, mutations at positions M307, M309 and L311 of PapG reduced PapG–PapF complex stability (i.e. a lower temperature was required for the complete dissociation of the variant PapGs from PapF relative to the wild-type adhesin), whereas mutations at position F313 had little or no effect on PapG–PapF interactions. Since the side chains at every other position in a β-strand are oriented in the same direction, these results suggest that the side chains of PapG residues 307, 309 and 311 constitute part of a continuous assembly surface that interacts with a complementary assembly surface on PapF. The absence of any discernible effect at

Table I. Effects of PapG C-terminal mutations

PapG variant	PapF–G complex stability[a]	PapD binding[b]
Wild-type	■■■■	●●●●
M307S	■■■	●
M307T	■■■	●
M307P	N/A	●●
M309A	■■■■	●
M309S	■	●
M309P	N/A	●
L311A	■■■	●
L311S	■■	●
L311T	■■■	●●
F313G	■■■■	●
F313L	■■■■	●●●
F313M	■■■■	●●●
F313A	■■■■	●
F313V	■■■■	●●
F313N	■■■■	●

[a]Relative stability of PapG–PapF interaction compared with wild-type PapG, as measured by the temperature required to achieve complete dissociation of PapG–PapF complexes. Each block (■) represents the number of temperature increments (shown in Figure 2B) above 42°C required for complete dissociation [e.g. four blocks indicate that all PapG ran as a monomer by lane 8 (71°C)]. 'N/A' signifies that enough material could not be purified from the specified construct in order to perform the experiment.
[b]Relative binding to PapD compared with wild-type PapG, as measured by ELISA using a PapG–MBP fusion protein. Each dot (●) represents ~25% binding capacity of wild-type at the highest concentration studied.

position 313 despite the array of substitutions explored suggests that this site is not critical for PapG–PapF interactions, although it may still contribute to the subunit–subunit interface. The requirement that cells be able to produce intact tip fibrillae for purification precluded the use of this assay to study the effects of mutations in the C-terminal region of the other tip subunits, PapE and PapF; the former is the main component of the tip polymer, while the latter has been shown to be required for the nucleation of tip assembly (Jacob-Dubuisson *et al.*, 1993).

We also examined the effects of these mutations on PapG–PapD interactions using an *in vitro* enzyme-linked immunosorbent assay (ELISA). Maltose-binding protein–PapG fusions (MBP–$PapG_{140}$) were constructed where the C-terminal 140 amino acids of PapG, containing each of the C-terminal variants, were fused to the C-terminus of MBP. The wild-type MBP–$PapG_{140}$ fusion has been shown previously (via this assay) to bind PapD with affinity roughly equal to that of full-length PapG (Xu *et al.*, 1995). In general, mutations at positions M307, M309, L311 and F313 of the PapG construct significantly reduced PapD binding (Table I). This finding is consistent with the observation that these mutations in PapG also led to a decrease in the levels of the adhesin incorporated into pilus tips (data not shown). Elimination of the last 14 residues from the MBP–$PapG_{140}$ fusion protein abolished PapD binding, as expected. An MBP–lacZα fusion construct also did not interact with PapD and served as a negative control. These results are consistent with the crystallographic data from the PapD–PapG-peptide complex, as well as with NMR data on the binding of PapD to an 8mer PapG C-terminal peptide and with studies using peptides as inhibitors of complex formation between PapD and MBP–$PapG_{140}$ (Karlsson *et al.*, 1998). It should be noted that it is possible that the non-conserved hydrophilic residues may also play an important role in pilus assembly. It might even be that one side of the strand interacts with the chaperone and the other side is involved in the assembly of the pilus, but the exact nature of these interactions awaits further analyses.

Effect of C-terminal mutations on the incorporation of PapA into the growing pilus

To investigate further the role of the C-terminus in mediating subunit–subunit contacts, we examined the effects of mutations within PapA, the major component of the pilus rod, with respect to pilus assembly. We selected G150 and Y162 as the targets for site-directed mutagenesis, as these two highly conserved positions flank the conserved C-terminal motif. Sites within this region (i.e. positions 151–161) were avoided intentionally because these would also affect PapA–PapD interactions (as deduced from the results with PapG), which would significantly cloud the interpretation of any observed changes with respect to pilus assembly.

Each of the PapA mutants was expressed *in trans* with a Δ*papA* (*papHCDJKEFG*) operon. Pili from each of the isogenic strains were purified via $MgCl_2$ precipitation and examined by SDS–PAGE (Figure 3A, lanes 6–8). Cells expressing either wild-type PapA or G150A-PapA produced pili as detected via the $MgCl_2$ purification procedure. In contrast, no pili could be isolated from cells expressing the G150T- or Y162L-PapA variants, indicating that these mutations abolished the ability of PapA to be assembled into rods.

Since stable PapD–PapA complexes can be isolated from strains expressing these latter two variants (Bullitt *et al.*, 1996), the absence of rods must have arisen as a consequence of either: (i) the inability of any PapA molecules to become incorporated into the growing organelle following the assembly of the tip fibrillum; or (ii) the inability of additional PapA subunits to assemble into a pilus rod subsequent to the incorporation of the first (or the first few) PapA subunit attached to the base of the tip fibrillum. In order to distinguish between these two possibilities, adhesive organelles expressed from these strains were purified via Gal-α(1,4)-Gal affinity chromatography and examined by both SDS–PAGE and high-resolution electron microscopy. This purification scheme relies on the tip-located PapG to bind to the receptor. In the case of wild-type pili, the tip fibrillum is joined to the adhesin and the rod is joined to the tip fibrillum, so the entire composite organelle was purified by this procedure as verified by quick-freeze deep-etch electron microscopy (Figure 3B, panel 1). Analysis of this material by SDS–PAGE revealed the presence of the PapA protein (Figure 3A, lanes 2, 6 and 10). In the absence of PapA, only tip fibrillae were purified (Figure 3B, panel 4) and analysis by SDS–PAGE revealed the lack of a PapA band (Figure 3A, lanes 5, 9 and 13). In the cases of the G150T and Y162L variants, only tip fibrillar structures were purified (Figure 3B, panels 2 and 3). However, examination of this material by SDS–PAGE revealed that the fibrillar structures contained PapA (Figure 3A, lanes 3–4, 7–8 and 11–12). Interestingly, small 'knobs' could be observed at the ends of many of the G150T- and Y162L-derived tips (not seen in the negative control), perhaps representing a

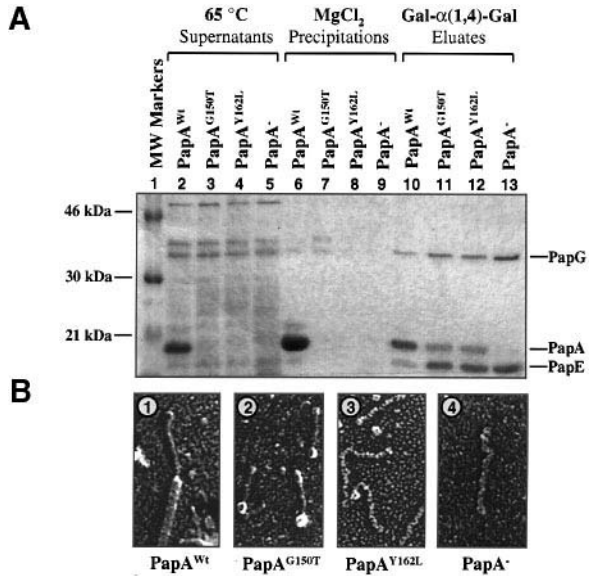

Fig. 3. (**A**) Crude extracts of surface tips/pili from strains expressing a *papA* gene encoding a C-terminal mutant *in trans* with a *papHCDJKEFG* operon were prepared and analyzed by SDS–PAGE (lanes 2–4). Pili could be purified via $MgCl_2$-induced cross-linking of PapA rods from a strain expressing wild-type PapA, but not from strains expressing the G150T or Y162L mutants (lanes 6–8). Affinity purification of tips/pili expressed from these strains was conducted by applying samples to a slurry of Gal-α(1,4)-Gal–Sepharose beads. After extensive washing, the bound PapG-containing structures (i.e. tips and pili) were eluted specifically with ethyl-β-galabioside. Examination of these samples by SDS–PAGE revealed that some PapA molecules were in fact incorporated into the growing organelles (lanes 10–12). Lanes 5, 9 and 13 contain samples prepared from an isogenic strain lacking *papA*. The PapA subunits were visualized by either Coomassie Blue staining (shown) or Western blotting with α−$PapDA_2$ antiserum. (**B**) Examination of the Gal-α(1,4)-Gal-purified structures by high-resolution EM revealed full-length pilus rods in the cases of wild-type PapA (panel 1), but only tip fibrillae in the cases of the G150T and Y162L mutants and the PapA deletion construct (panels 2, 3 and 4). Interestingly, small 'knobs' could be observed at the ends of many of the G150T- and Y162L-derived tips (not seen in the negative control), perhaps representing a partial helical turn of one or more PapA molecules.

partial helical turn of one or more of the incorporated PapA molecules.

Structure of PapD–PapK-peptide complex

In order to investigate the extent to which PapD caps the PapA C-terminal assembly surface, we attempted to co-crystallize PapD with a 19mer C-terminal PapA peptide, but solubility problems with the peptide hampered these attempts. However, we were successful in co-crystallizing PapD with a 19mer peptide corresponding to the C-terminal region of PapK, which possesses the same side chains within the conserved alternating hydrophobic motif as PapA (Tyr2′, Leu4′, Phe6′ and Ala8′, where the number denotes the residue's position relative to the C-terminus).

The crystal structure of the PapD–PapK-peptide complex was solved to 2.8 Å resolution (Figure 4). Crystal data and refinement parameters are summarized in Table II. The peptide bound in an extended conformation along the outer G1 β-strand of PapD via a β-zipper motif comprised of seven main chain hydrogen bonds between the peptide and the G1 β-strand; this interaction effectively extended the β-sheet formed by PapD's G1, F1, C1 and D1 β-strands out to a fifth strand. The C-terminus of the peptide was anchored in the interdomain cleft of PapD by hydrogen bonds to the side chains of Arg8 and Lys112.

The Arg1′ side chain of the peptide made several van der Waals contacts with residues from domain 2 of PapD: Ile154, Thr170 and Ile194. All other contacts between the peptide and PapD involved residues from domain 1 of the chaperone. The side chain of the highly conserved Tyr2′ made limited van der Waals contact with the shallow pocket formed by PapD residues Leu4, Thr7, Thr109 and Ile111; interestingly, the hydroxyl group of the peptide's Tyr2′ side chain did not appear to hydrogen-bond with any residues of PapD. This suggests that while the conserved aromatic moiety might be important for chaperone binding, as deduced from the ELISA results above, the hydroxyl group might play a role in mediating subunit–subunit interactions. Indeed, substitution of Phe for the penultimate Tyr in PapA has been shown to alter the helical symmetry of the pilus rod (Bullitt *et al.*, 1996). Additional van der Waals contacts with PapD were made by the side chains of Leu4′ and Ala8′, which are part of the conserved hydrophobic motif common to all pilus subunits; these made contact with the side chains of Ile105 and Leu107 from the conserved G1 β-strand of PapD (Figure 5).

The first five N-terminal residues of the peptide displayed no electron density, and must therefore have been disordered in the crystal structure. Overall, these observations are in general agreement with the interactions seen in the previously determined crystal structure of the PapD–PapG-peptide complex, although the peptide side chains at positions 2′ and 6′ appear to make notably less extensive contacts with the chaperone. Remarkably, superimposition of the ligands from the PapD–PapG- and PapD–PapK-peptide crystal structures revealed that they adopt a virtually identical amide backbone conformation in the region that interacts with the G1 β-strand of PapD, despite the fact that side chain identities differ at 15 out of the 19 positions. This underscores the importance of the hydrogen bonding interactions comprising the β-zipper motif.

Additional insight was gained through a comparison of the PapD structures from these two complexes as well as from the apo-PapD crystal structure (Holmgren and Brändén, 1989). The complete PapD C_α traces from all three crystal structures, as well as sectional C_α traces from selected regions of PapD, were superimposed, and positional root-mean-square deviations (r.m.s.ds) for corresponding atoms were calculated (Table III). This analysis revealed that only modest conformational changes occur upon peptide binding, except within the loop region connecting the F1 and G1 β-strands (Figure 6; Table IV). Here, a substantial degree of ordering occurs upon ligand binding that extends the apparent length of the G1 β-strand as defined by the corresponding Φ and Ψ torsion angles of the polypeptide backbone within this region. It was previously unknown if the changes in conformation of the F1–G1 loop seen in the PapD–PapG-peptide crystal structure were a result of ligand binding or only a consequence of crystal packing. The similar conformational changes seen in the PapD–PapK-peptide structure strongly argue that the reorganization of this region and the resulting elongation of the G1 β-strand are due in fact to peptide binding.

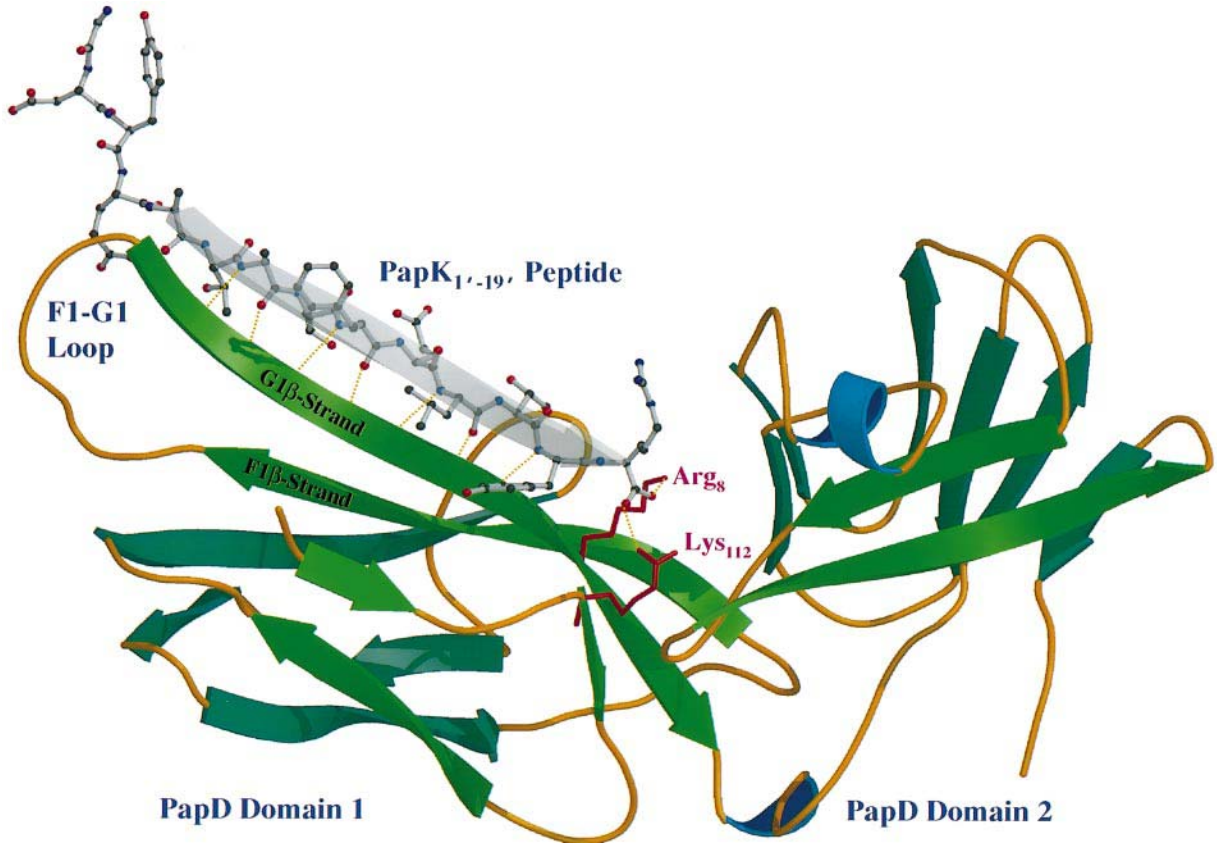

Fig. 4. Ribbon representation of the PapD–PapK-peptide crystal structure showing the peptide bound in an extended conformation along the G1 β-strand of PapD, effectively extending the β-sheet defined by strands G1, F1, C1 and D1 of PapD. The peptide is bound via a β-zipper motif comprised of main chain hydrogen bonds. The C-terminus of the peptide is anchored in the interdomain cleft by additional hydrogen bonds to Arg8 and Lys112 of PapD. A translucent β-strand is drawn through the K-peptide. The figure was generated using MOLSCRIPT (Kraulis, 1991) and Raster3D (Bacon and Anderson, 1988; Merritt and Murphy, 1994).

Table II. Crystal data and refinement parameters

Space group	C2221
Unit cell (Å)	
a	57.20
b	153.77
c	135.86
α = β = γ	90°
Resolution (Å)	2.8
Percent complete (20–2.8 Å)	95.5
Percent complete (2.9–2.8 Å)	85.1
Protein atoms	3428
Ligand atoms	232
Total reflections	16 071
R.m.s.d. bond (Å)	0.019
R.m.s.d. angle	3.87°
R_{sym} [a]	0.075
R_{cryst} [b]	0.192

[a]$R_{sym} = \Sigma_h\Sigma_i|I_{hi} - <I_h>|/\Sigma_h\Sigma_i I_{hi}$, where I_{hi} and I_h are the intensities of the individual and mean structure factors, respectively.
[b]$R_{cryst} = \Sigma|F_{obs} - F_{calc}|/\Sigma F_{obs}$, where F_{obs} and F_{calc} are observed and calculated structure factor amplitudes, respectively. Only data with $F_{obs}/\sigma(F_{obs}) > 2.0$ were used in the refinement.

The total buried surface area between the peptide and protein is 621 Å^2, a value similar to that of 582 Å^2 seen in the PapD–PapG-peptide crystal structure. This represents a relatively small value when compared with other known intermolecular contact interfaces between proteins of similar size (Jones and Thornton, 1995; Stites, 1997). This observation suggests that the C-terminal region of pilus subunits may only represent part of the chaperone recognition motif. The other highly conserved region of pilus subunits is located near their N-termini (Figure 1B) (Normark *et al.*, 1986; Hultgren *et al.*, 1996). Given the ability of periplasmic chaperones to form complexes with an array of different subunits, one would speculate that the chaperone recognition motif would be highly conserved (Kuehn *et al.*, 1993). Thus the conserved N-terminal region found in most pilus subunits could serve as a putative 'second site' or an extension of a single, more expansive chaperone-binding motif than defined by the C-terminal region alone (Hultgren *et al.*, 1996; Jones *et al.*, 1996). We therefore constructed a set of PapA variants with point mutations in this region and characterized them with respect to their ability to form chaperone–subunit complexes and to be assembled into pili.

Effect of N-terminal mutations on chaperone–subunit and subunit–subunit interactions

To probe the role of the conserved N-terminal region of pilus subunits with respect to chaperone binding, we constructed variants of PapA with single substitutions at various interspersed positions between sites 11 and 31. The effects of these substitutions on the formation of PapD–PapA complexes are shown in Figure 7A. Mutations at positions I24 and Q31 abolished the formation of heterodimeric PapDA complexes but did not prevent heterotrimeric $PapDA_2$ complex formation (levels of

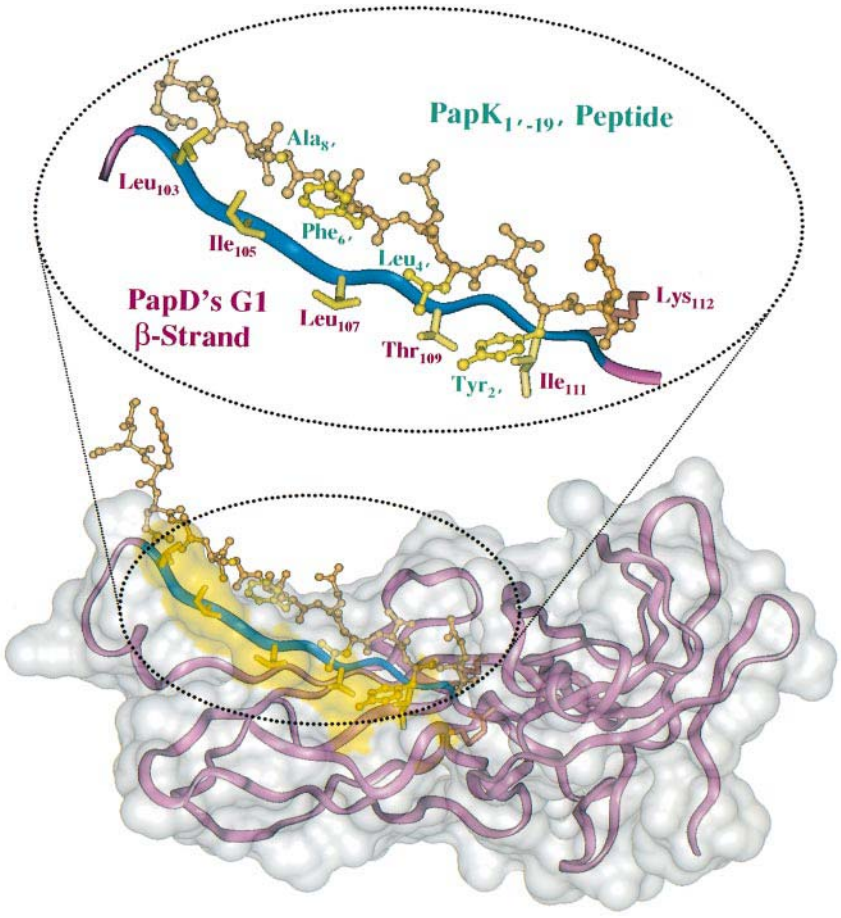

Fig. 5. Ribbon representation of the PapD–PapK-peptide crystal structure, shown here with PapD's solvent-accessible connolly surface. The hydrophobic bed comprised of residues along PapD's G1 β-strand is highlighted in yellow. The inset provides a magnified view of the PapD–PapK-peptide contact interface. Note how the conserved alternating hydrophobic residues of the peptide interdigitate with the residues along PapD's G1 β-strand. The figure was generated using the Insight II modeling package (MSI, San Diego, CA).

Table III. Superimposition of PapD C_α traces from the apo-PapD structure and PapD–PapG/K-peptide complexes

Molecules superimposed	R.m.s.d. (Å)				
	Entire molecule[a] (residues 1–218)	Domain 1 (1–115)	Domain 1[b] (1–80)	Domain 1[b] (81–115)	Domain 2 (125–218)
PapDK on PapDG	0.927	0.948	0.429	1.374	0.557
PapD on PapDK	1.603	2.026	0.391	2.718	0.530
PapD on PapDG	1.694	1.855	0.449	2.526	0.646

[a]See Figure 6A.
[b]See Figure 6B and C.

$PapDA_2$ complex were decreased in the Q31 variant). Similar results were reported previously when mutations were introduced at position Y162 of PapA, presumably as a consequence of the disruption of the chaperone recognition motif (Bullitt *et al.*, 1996). Ternary complex formation evidently is still favored, however, presumably through a stabilizing interaction involving the second PapA subunit; this interaction may bridge another subunit-binding region of PapD with a second distinct assembly surface on the first PapA molecule (Bullitt and Makowski, 1993; Bullitt *et al.*, 1996).

We subsequently examined the ability of these N-terminal variants to become assembled into pili (Figure 7B). Strains expressing PapA mutants with substitutions at positions F13, G15, V17, I24 and Q31 were unable to produce $MgCl_2$-precipitable pili (Figure 7B, lanes 7–11, and data not shown), suggesting that these residues contribute to an assembly surface that mediates PapA–PapA interactions in the pilus rod. We examined selected constructs that did not produce pili for their ability to become incorporated into the growing organelle by probing for PapA protein in tips purified by Gal-α(1,4)-Gal affinity chromatography (Figure 7B, lanes 13–17). Analysis of these tips from strains expressing these constructs by SDS–PAGE revealed the presence of the PapA protein; hence, as with the C-terminal constructs, these

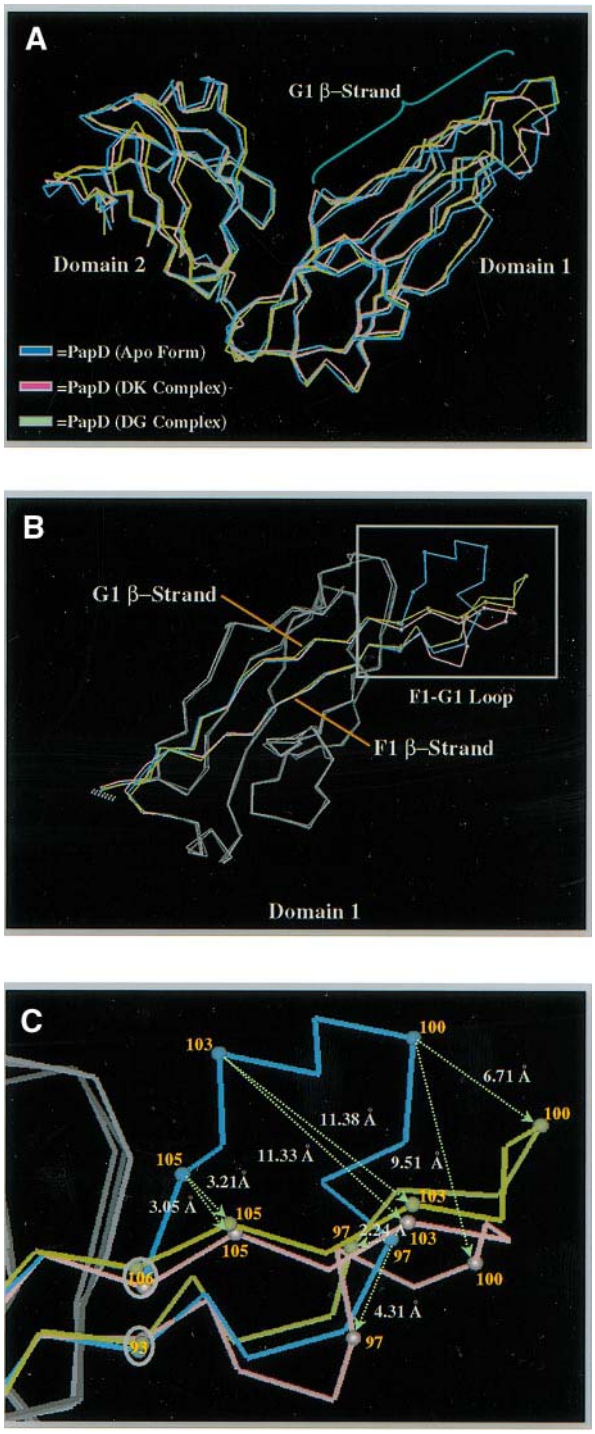

Fig. 6. (**A**) Superimposition of the C_α traces from the unbound and peptide-bound forms of PapD. (**B**) Superimposition of the C_α traces from domain 1 of the unbound and peptide-bound forms of PapD. Examination of the superimposed molecules revealed only modest conformational changes upon peptide binding, except within the F1–G1 mobile loop (Table IV). PapD residues 102–105 shift from their positions in the unbound form so as to extend the apparent length of the G1 strand upon binding of the peptides. (For this figure, the C_α traces of residues 1–80 from domain 1 were used to align the structures.) (**C**) Close up of the boxed region in (B). Residue numbers are indicated next to the appropriate C_α. The shifts in a given C_α's position upon ligand binding are given by the interatomic vectors.

mutant PapAs could also be incorporated into the growing organelle, although subsequent elongation of the pilus rod is aborted.

Table IV. Interatomic distances between residues in the F1–G1 loop region

Position	Interatomic distances between corresponding C_αs (Å)		
	DK and DG	D and DK	D and DG
Ile93	0.29	0.49	0.47
Pro94	1.13	0.47	0.79
Pro95	1.20	0.61	0.84
Arg96	3.14	2.65	0.81
Ser97	3.38	4.31	2.24
Glu98	3.21	3.21	2.97
Lys99	4.58	5.56	4.31
Ala100	5.63	9.51	6.71
Asn101	2.95	11.55	10.16
Val102	1.52	11.53	10.19
Leu103	0.86	11.33	11.38
Gln104	1.12	6.85	6.93
Ile105[a]	1.14	3.05	3.21
Ala106[a]	0.90	0.80	0.84
Leu107[a]	0.48	0.20	0.44
Gln108[a]	0.44	0.39	0.22

[a]Part of G1 β-strand.

Effect of second site mutations on chaperone–adhesin interactions

Adhesins such as PapG lack the conserved N-terminal region found in other subunits. However, Xu *et al.* (1995) demonstrated that PapD specifically recognizes a peptide corresponding to residues 170–195 of the PapG adhesin (the so-called 'second site' peptide, as its binding was shown to be independent of the binding of the PapG C-terminal peptide). This region of PapG corresponds in approximate sequence position (as measured from the C-terminus) to the highly conserved N-terminal region of other pilus subunits (Figure 8A). We therefore explored the effects of mutations in this region of PapG with respect to PapD–PapG complex formation and stability (Figure 8B).

Periplasms were obtained from strains co-expressing wild-type PapD with each of the PapG variants and examined by SDS–PAGE and Western blotting using α-PapD/PapG antibodies. A mutation at position 184 of PapG abrogated its ability to bind and form a stable complex with PapD. Furthermore, this mutation led to the appearance of a low molecular weight band, identified by N-terminal sequencing as a truncate of PapG. Such truncates have been seen in previous studies using PapG constructs in which the C-terminal chaperone recognition motif has been deleted, and is indicative of PapD's inability to bind the variant subunits and confer upon them protection from proteolysis (Hultgren *et al*., 1989).

Discussion

Molecular chaperones represent a diverse set of proteins involved in various biological pathways in both prokaryotic and eukaryotic cells. Although significant differences exist with respect to the structure of these proteins and the mechanisms by which they function, they ultimately serve a common purpose: the prevention of non-productive interactions during the folding or assembly of a protein or protein complex. Much progress has been made towards elucidating the molecular basis of how various cytoplasmic

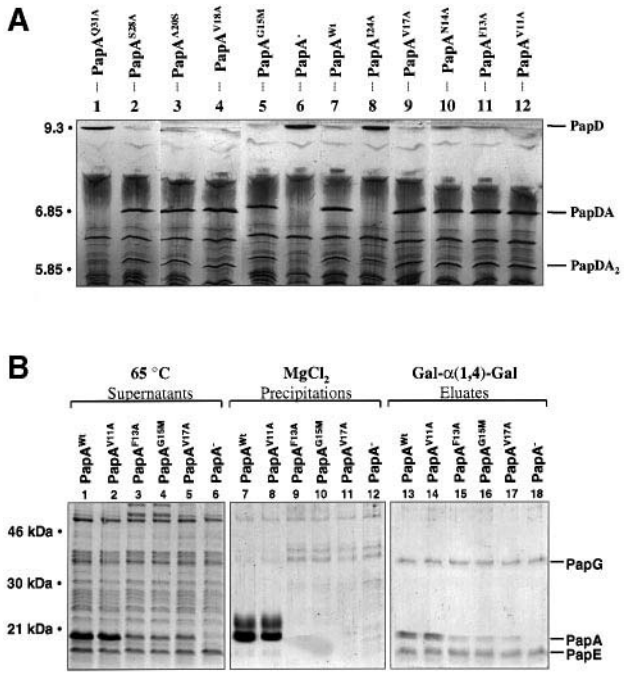

Fig. 7. (**A**) Silver-stained isoelectric focusing gel electrophoresis demonstrating PapDA (1:1) and $PapDA_2$ (1:2) complexes. PapD, PapDA and $PapDA_2$ migrate to well-characterized positions on isoelectric focusing gels (Jacob-Dubuisson *et al.*, 1994b; Striker *et al.*, 1994). Note that substitution of I24 or Q31 abolishes the formation of the PapDA complex. (**B**) Crude extracts of surface tips/pili from strains expressing a *papA* gene encoding an N-terminal mutant *in trans* with a *papHCDJKEFG* operon were prepared and analyzed by SDS–PAGE (lanes 1–5). Pili could be purified via $MgCl_2$-induced cross-linking of PapA rods from a strain expressing wild-type PapA and the V11A variant, but not from strains expressing F13A, G15M or V17A variants (lanes 7–11). Strains expressing the N14A, V18A, A20S and S28A variants were also able to produce $MgCl_2$-precipitable pili, whereas the I24A and Q31A variants were unable to assemble rods (data not shown). Affinity purification of tips/pili expressed from these strains was conducted by applying samples to a slurry of Gal-α(1,4)-Gal–Sepharose beads. After extensive washing, the bound PapG-containing structures (i.e. tips and pili) were eluted specifically with ethyl-β-galabioside. Examination of these samples by SDS–PAGE revealed that some PapA molecules were in fact incorporated into the growing organelles (lanes 13–17). Lanes 6, 12 and 18 contain samples prepared from an isogenic strain lacking *papA*. The PapA subunits were visualized by either Coomassie Blue staining (shown) or Western blotting with α−$PapDA_2$ antiserum.

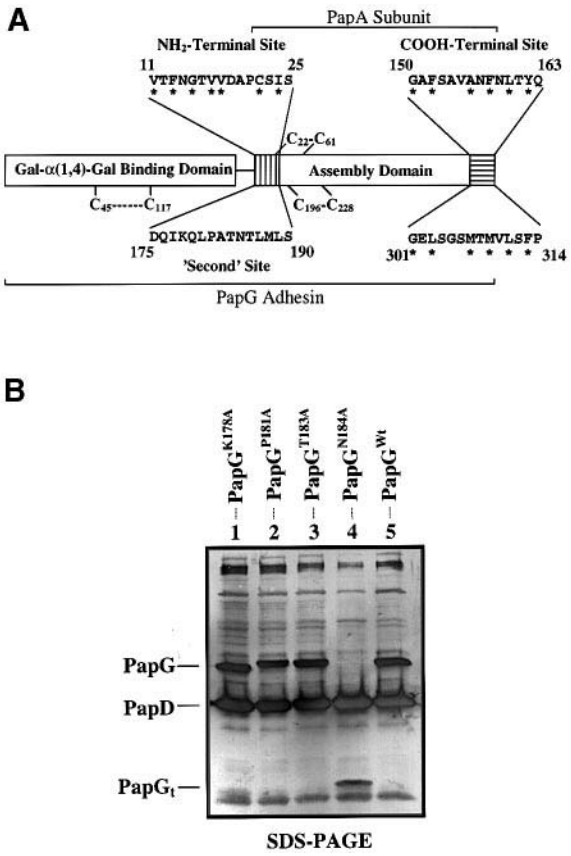

Fig. 8. (**A**) A composite schematic of a pilus subunit, PapA, and a pilus adhesin, PapG, showing the conserved features of pilus subunits. The C-terminal motif of alternating hydrophobic residues is present in all pilus subunits, while the N-terminal hydrophobic motif is present in all non-adhesin subunits. Conserved positions are marked by an asterisk (*). (**B**) SDS–PAGE of periplasms from strains expressing PapD together with wild-type PapG or variants of the adhesin containing point mutations within the second site region. Substitution at position 184 abolished PapD–PapG complex formation and led to proteolytic truncation of PapG. PapG and PapD were visualized by Western blotting with α-PapDG antiserum.

chaperones function. However, only now are the details of periplasmic chaperone function beginning to emerge at the same level of resolution.

In this study, we begin to shed light on the mechanism by which periplasmic chaperones prevent the premature oligomerization of folded subunits in the periplasmic space by developing a more detailed picture of the subunit interactions responsible for maintaining the quaternary structure of the pilus. Two types of subunit assembly surfaces are thought to exist: (i) primary assembly surfaces, which are involved in mediating interactions between linearly adjacent subunits in the pilus fiber; and (ii) secondary packing surfaces, which are involved in mediating contacts between subunits located in adjacent turns of the pilus rod. Primary assembly surfaces are present in all subunits comprising the pilus fiber, and are involved in the 'head-to-tail' interactions that join neighboring subunits together in the contiguous fiber (i.e. the head of the *n*th subunit is attached to the tail of the *n*th – 1 subunit, where $n = 1$ is the index for the distal-most subunit at the tip. Secondary assembly surfaces are unique to PapA, and account for the ability of the PapA polymer to be packaged into a hollow cylinder with a right-handed helical symmetry of 3.3 subunits per turn (Gong and Makowski, 1992; Bullitt and Makowski, 1993). Under appropriate conditions, these secondary packing interactions can be disrupted, resulting in the pilus rod adopting an extended linear conformation (Bullitt and Makowski, 1993; Thanassi *et al.*, 1998).

The lack of any structural information at the atomic level of resolution for these macromolecular assemblies has been a limiting factor in the determination of what residues are important for mediating subunit contacts within the pilus. Herein, we have used genetic and biochemical techniques to show that the conserved C-terminal motif of two structurally distinct subunits, the PapG adhesin and the PapA subunit, maps to a primary assembly surface. In the case of PapG, we demonstrated that mutations at three of the four residues comprising the C-terminal motif of alternating hydrophobic residues have a direct impact on the stability of PapG–PapF interactions

in the assembled pilus tip. With PapA, we showed that mutations at positions flanking this C-terminal motif limit or abolish PapA–PapA interactions, but not PapA–PapK interactions during pilus biogenesis. These results suggested that the C-terminal region of subunits constitutes part of the 'tail' assembly surface, since in these variants PapA's ability to recognize a complementary surface on the preceding subunit in the pilus (e.g. PapK) is retained, whereas its ability to interact with the next incoming PapA subunit in the rod is abolished. This conclusion is consistent with PapG's position at the distal end of the pilus, as it would not be expected to possess a 'head' assembly surface. The direct capping of a primary assembly surface, therefore, is apparently part of the molecular basis by which periplasmic chaperones prevent the premature oligomerization of pilus subunits.

A comparison of the newly solved PapD–PapK-peptide structure with that of the PapD–PapG-peptide complex proved most revealing. Despite substantial sequence differences between the G- and K-peptides, the amide backbones of the two ligands are virtually superimposable in the region that interacts with the G1 β-strand of PapD, emphasizing the importance of the hydrogen bonding interactions comprising the β-zipper motif. An important question that arises from these structures is whether or not the β-zipper motif is sufficient for chaperone–subunit recognition, and does it represent the entire contact interface between subunit and chaperone? The total amount of surface area buried upon peptide binding is <625 Å^2 for both complexes. Jones and Thornton (1995, 1996) recently surveyed all non-homologous oligomeric structures in the Brookhaven Protein Data Bank and found that the size of protein–protein interfaces ranged from 368 to 4746 Å^2 for homodimers and from 639 to 3228 Å^2 for heterocomplexes. They also noted a positive linear relationship between interface size (A_i) and protomer molecular weight (M_r), with $A_i = 0.06\ M_r$ (the correlation coefficient of the 32 data points to this model was 0.69). For a PapD–PapG complex with a molecular weight of 60 kDa, this relationship predicts an interface size of ~1800 Å^2. The observed interface between PapD and the C-terminus of a subunit is much smaller than this predicted value, although it does fall within the tail end of the experimentally observed distributions of other complexes. We therefore explored the possibility of additional contact surfaces between the pilus subunits and chaperone.

We focused on the only other highly conserved region of pilus subunits located near the N-terminus, speculating that it may also constitute a portion of the chaperone recognition motif (Kuehn *et al.*, 1993). We found that mutations within the N-terminal region of PapA spanned by residues 11–20 had no observable effects on periplasmic levels of PapDA or $PapDA_2$ complexes. However, mutations further downstream at positions 24 and 31 decreased complex formation with PapD, although it is not clear whether this was due to a specific destabilizing effect at the PapD–subunit interface or an effect on the PapA subunit as a whole. In the corresponding region of the PapG adhesin, we found a mutation that destabilized the interactions with the chaperone and resulted in proteolytic truncation of PapG. These results are consistent with a model in which the chaperone recognizes a second binding motif of pilus subunits located ~130 residues upstream from a subunit's C-terminus—a model which is strongly supported by the binding of the PapG(170–195) 'second site' peptide to PapD as previously reported by Xu *et al.* (1995). Attempts to find N-terminal peptides of PapA that bind PapD have so far been unsuccessful. This may be due to the occurrence of a disulfide-bonded cysteine located within the conserved N-terminal region (the corresponding cysteine in PapG lies just downstream of the second site region); without the disulfide bond, short synthetic peptides may not be able to adopt the appropriate conformation needed for PapD recognition. This is consistent with *in vivo* results indicating that DsbA-catalyzed disulfide bond formation in pilus subunits appears to occur prior to formation of chaperone–subunit pre-assembly complexes (Jacob-Dubuisson *et al.*, 1994b). It is interesting to note that with respect to subunit–subunit interactions, substitutions in the N-terminal alternating hydrophobic motif of PapA (e.g. positions 13, 15 and 17) had the same discernible effect on rod formation as their C-terminal counterparts. This suggests that the conserved N- and C-terminal regions may play a similar role in the quaternary structure of the pilus rod (i.e. these two regions may be juxtaposed in the three-dimensional structure of the subunit and could both be part of the same surface). Alternatively, the N-terminal region may function as the 'head' assembly surface of the *n*th subunit that interacts with and is complementary to the C-terminal 'tail' assembly surface of the *n*th – 1 subunit. This would explain why this region is so conserved across all pilus subunits except in the adhesins, which form the starting point for the pilus fiber. Either model is consistent with the observation that mutations in the N-terminal motif of PapA abolish pilus rod formation. Furthermore, the detection of PapA in preparations of affinity-purified tips may reflect lateral or secondary packing interactions that could help stabilize incoming PapA molecule(s) even in the face of a substitution that partially disrupts the primary contact interface. Therefore, it is not possible at this time to define unambiguously the context of the conserved N-terminal region in the quaternary structure of the pilus, although the available evidence seems to indicate that the surface defined by this motif of alternating hydrophobic residues is involved directly in mediating subunit–subunit contacts.

A careful analysis of all crystallographic data on PapD available to date provides some additional insight into other aspects of periplasmic chaperone function. Circular dichroism (CD) studies have revealed that pilus subunits are predominantly β-sheet proteins (S.J.Hultgen, unpublished results). Jones *et al*. (1997) have demonstrated that nascent subunits destined for incorporation into the pilus initially are retained by the inner cytoplasmic membrane in an unfolded state following their translocation into the periplasmic space. In the absence of the chaperone, the subunits enter a non-productive pathway and are degraded. In the presence of the chaperone, these nascent subunits continue along the assembly pathway through chaperone-mediated extraction from the inner membrane, folding into an assembly-competent conformation and delivery to the outer membrane assembly site.

The crystal structures of the PapD–PapG- and PapD–PapK-peptide complexes afford insight into the molecular mechanism by which subunit extraction from the inner membrane occurs by providing what might be considered

a 'snap-shot' of the initial interactions between the chaperone and a subunit (Kuehn *et al.*, 1993). The retention of nascently translocated subunits by the inner cytoplasmic membrane is mediated by their hydrophobic C-termini (Jones *et al*., 1997). It is likely that the C-termini of the subunits adopt an α-helical conformation when membrane associated. This is supported by CD studies performed using synthetic peptides corresponding to the C-termini of various subunits (e.g. PapG, PapK, PapE and PapF) that demonstrated that these sequences adopt a significant degree of α-helical structure within a hydrophobic environment (Karlsson *et al*., 1996). This model is consistent with the known tendencies of peptides containing a high fraction of hydrophobic residues, and in particular aromatic residues, to partition into a lipid bilayer interface as α-helical structures in order to satisfy the backbone's hydrogen bonding capacity (Engelman and Steitz, 1981; Derber and Goto, 1996; Wimley and White, 1996). Although the initial point(s) of contact between the chaperone and subunit is unknown, the highly conserved N-terminal region, which as we have shown in this study is recognized by the chaperone and presumably is exposed in the periplasm following translocation, is an attractive candidate. Once the chaperone is bound to the subunit and localized to the membrane, subsequent steps would include partitioning of the subunit's C-terminus out of the membrane, its anchoring in the cleft of the chaperone and formation of the β-zipper. The critical role of the anchoring interaction has been demonstrated previously by the inability of Arg8 and Lys112 variants of PapD to form chaperone–subunit complexes *in vitro* or assemble pili *in vivo* (Slonim *et al.*, 1992; Kuehn *et al.*, 1993).

Once cleared from the inner membrane, the subunits are free to fold into an assembly-competent (native) state. The precise role that PapD plays in the folding of subunits has yet to be elucidated. One can envision a kinetic role for PapD in the folding pathway in which the β-zipper motif could provide a pre-defined context in the form of a template for initial β-strand formation. Several experimental and theoretical studies have demonstrated that β-structure formation can be a slow step in the folding pathway of a protein, and that it is often context dependent (Finkelstein, 1991; Minor and Kim, 1994; Hamada *et al.*, 1996). This context-driven model of subunit folding is particularly intriguing in light of the conformational changes seen in the F1–G1 loop region, and the finding by Hung and co-workers that members of the periplasmic chaperone superfamily may be divided into two structural and functional classes based on the length of this loop region (Hung *et al.*, 1996). The FGS chaperones possess short loops ranging in size from 10 to 20 residues and are involved in the assembly of rod-like pili. The FGL chaperones have longer loops ranging in size from 21 to 29 residues and assemble non-pilus organelles. It has been speculated that differences in the length and sequence of the F1–G1 loop might provide part of the specificity in chaperone–subunit interactions (Kuehn *et al.*, 1993; Hung *et al.*, 1996). However, the observed conformational changes that occur upon binding may also provide insight into the molecular basis for how differences in the length of this region correlate with different adhesive organelle morphologies. As previously noted, a substantial degree of ordering occurs upon ligand binding that extends the apparent length of the G1 β-strand as defined by the corresponding Φ and Ψ torsion angles of the residues within this region. With their longer loop regions, FGL chaperones have the potential for forming more extensive β-strand templates. Such extended templates could be important in the folding of subunits that form afimbrial adhesins.

Alternatively, PapD may function by binding to aggregation-prone intermediates along a subunit's folding pathway. In this role, PapD would not necessarily alter the kinetics of folding along this pathway. Rather, interaction with PapD effectively would enhance the yield of native subunits by protecting aggregation-prone species from interacting with one another and partitioning subunits towards a folded state. This may indeed be an important mechanism given the environment of the periplasmic compartment, where protein concentrations are thought to be quite high (Oliver, 1996).

Regardless of what mechanisms might be in play in chaperone-mediated folding of the subunits, once subunits have achieved a native-like conformation these chaperones must continue to prevent the quaternary structural interactions between individual pilus subunits from occurring prior to their delivery to the outer membrane assembly site. We have shown through mutations in two structurally distinct subunits, the PapG adhesin and the PapA rod-forming subunit, that the subunit's C-terminal region serves as an assembly surface mediating subunit–subunit interactions in addition to serving as a chaperone binding motif. The evolutionary advantages of this dual function are self-evident. The membrane can serve as a temporary repository for nascently translocated subunits. This scheme eliminates the need for critical timing of subunit import to the periplasmic side of the inner membrane with arrival of the chaperone at the site of import. By binding to the C-terminal region of the subunits, the chaperone is able to extract the subunit from the membrane. This extraction is coupled to the folding of the subunit polypeptide chain into an assembly-competent conformation, which creates the assembly surfaces involved in mediating subunit–subunit interactions in the final pilus structure. However, once formed, the C-terminal assembly surface remains protected by virtue of the fact that it remains bound by the chaperone. Hence, by coupling subunit folding and capping of an assembly surface, the periplasmic chaperones ensure that premature assembly interactions are prevented (Figure 9).

This mechanism of periplasmic chaperone function is distinct from that of the cytoplasmic chaperones and is well adapted to the problem of folding proteins destined for assembly into large polymers while at the same time preventing them from entering non-productive aggregation pathways. Like other molecular chaperone systems such as DnaK–DnaJ and GroEL–GroES, the periplasmic chaperones recognize unfolded or partially folded polypeptide substrates. As with the DnaK–DnaJ system, periplasmic chaperones bind to an extended motif of their substrates. However, this binding serves two very distinct roles in each of these systems. The interaction of a nascent polypeptide chain with DnaK and DnaJ serves to prevent the formation of otherwise kinetically favored misfolded intermediates; the substrate protein ultimately forms a native structure or is transferred for final folding to the

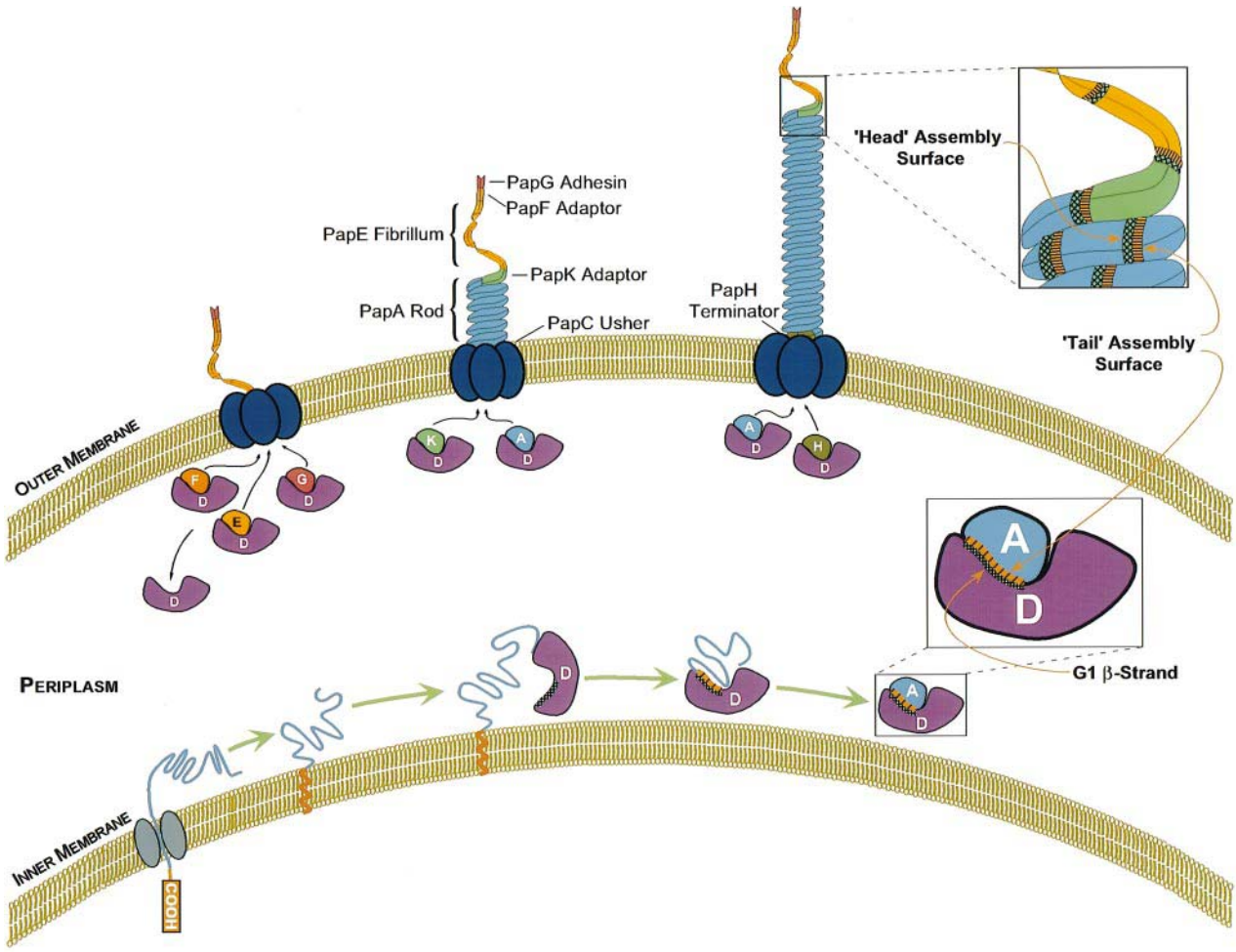

Fig. 9. Schematic representation of pilus assembly via the chaperone–usher pathway. Chaperone-mediated extraction of subunits from the inner cytoplasmic membrane is coupled with their folding into an assembly-competent state. The G1 β-strand of the immunoglobulin-like chaperones, which may serve as a template in the subunit folding pathway, protects nascently folded subunits from premature oligomerization in the periplasmic space by directly capping the newly formed assembly surfaces. These interactive surfaces remain protected by the chaperone until delivery of the pre-assembly complex to the outer membrane assembly site.

GroEL–GroES system. In the case of the periplasmic chaperones, binding of a nascent polypeptide chain to the G1 β-strand of the chaperone may facilitate its folding into a native-like conformation by protecting an aggregation-prone surface and/or providing a template to enhance the rate of folding. In this respect, the periplasmic chaperones are functionally analogous to the GroEL–GroES system in that they provide a protected 'environment' or 'context' for substrate folding. However, in contrast to either of the cytoplasmic chaperone systems, the periplasmic chaperones retain their substrates once they have attained their native-like conformations, protecting their interactive assembly surfaces from premature interactions until delivery to the pilus assembly site.

Another highly distinct feature of periplasmic chaperones is that their mode of action is essentially independent of cellular energy stores (Jacob-Dubuisson *et al.*, 1994a). Indeed, the self-assembly of subunits into pili appears to be driven thermodynamically by the formation of ternary subunit–subunit contacts, a model supported by the observation that PapA rods can be formed *in vitro* from purified PapD–PapA complexes that are morphologically indistinguishable from cell-isolated pili (Bullitt *et al.*, 1996). This independence from cellular energy stores and their multifunctional nature makes periplasmic chaperones very energetically economical, an important characteristic when one considers the large number of subunits a bacterial cell must synthesize during pilus biogenesis.

Materials and methods

Strains and genetic constructs

Escherichia coli strains HB101 (Boyer and Roulland-Dussoix, 1969), MC1061 (Lech and Brent, 1987) and KS474 (Strauch *et al.*, 1989) were used as the host strains for cloning, mutagenesis and expression. The plasmid pAC101 contains a *papA*$^-$ operon (*papHCDJKEFG*) under the control of the P_{trc} promoter and was created from pFJ29 (Jacob-Dubuisson *et al.*, 1993) by enzymatic cleavage at the *Hin*dIII restriction site in *papA*, followed by Klenow treatment and religation. The plasmid pKD320 (*papHCDJKEF*) is a *papG*$^-$ derivative of pAC101 made by insertion of a Tn*5* kanamycin resistance gene cassette (DasGupta *et al.*, 1987) into the *Bgl*II site of *papG*.

PapA variants under control of the P_{tac} promoter in pMMB66 derivative plasmids were created via PCR mutagenesis as described previously (Morrison and Desrosiers, 1993; Bullitt *et al.*, 1996) and were then transformed into HB101/pAC101 and HB101/pHJ9203 (Jones *et al.*, 1997) strains. PapG C-terminal variants under the control of the P_{tac} promoter in pLS201 (Slonim *et al.*, 1992) derivative plasmids were created by direct ligation of oligonucleotides (encoding the last 14 amino acids) containing the mutations between the available *Bam*HI and *Sma*I sites at the 3′ end of *papG*. These pLS201 derivatives were then

transformed into an HB101/pKD320 strain. PapG second site variants under the control of the P_{tac} promoter in pMMB66 derivative plasmids were created via PCR mutagenesis as described previously (Morrison and Desrosiers, 1993) and were then transformed into an HB101/pHJ9203 strain. Mutant MBP–$PapG_{140}$ fusion constructs were created by subcloning the *papG* mutant fragments obtained from the pLS201 derivative plasmids encoding the C-terminal mutants into pMAL/G175–314 (Xu *et al.*, 1995). All constructs were verified by dideoxy sequencing.

Heat stability assays of adhesin–adaptor complexes

MC1061 strains containing the PapG constructs were grown in Luria broth (pH 7.4) medium containing the appropriate antibiotics up to an optical density of 0.8 at 600 nm, prior to induction with 1 mM isopropyl-β-D-thiogalactoside (IPTG) for 60 min. Cells subsequently were spun down and resuspended in phosphate-buffered saline (PBS) and heated for 30 min at 65°C to extract surface tips. Aliquots of the tip suspensions were treated with SDS sample buffer and incubated at various temperatures from 25 to 95°C for 10 min. The samples were then analyzed by SDS–PAGE followed by Coomassie Blue staining or immunoblotting using rabbit α-PapG or mouse α-PapE as the primary antibodies, and ^{35}S-labeled α-rabbit IgG and alkaline phosphatase-conjugated α-mouse IgG as the secondary antibodies. This dual antibody technique was used so that PapG–PapF stability could be monitored by autoradiography with simultaneous monitoring of PapE levels using NBT and BCIP. None of the PapG mutant constructs affected PapE complex stability.

ELISA of PapD binding to MBP–$PapG_{140}$ fusion constructs

MBP–$PapG_{140}$ derivatives were purified as described previously (Xu *et al*., 1995). These preparations contained both full-length fusion proteins as well as various C-terminal truncates. Since it has been shown that MBP–$PapG_{140}$ truncates lacking the last 14 amino acids of the wild-type PapG sequence were unable to bind PapD, the amounts of full-length MBP–$PapG_{140}$ in the preparations were equalized prior to their use (as determined by SDS–PAGE, Coomassie Blue staining and densitometry). The normalized preparations were then coated overnight at 4°C in PBS onto Immunosorp plates at concentrations of 1.25, 2.5, 5, 10, 20 and 40 pmol/well. Plates were rinsed with PBS and then blocked with 3% (w/v) bovine serum albumin (BSA) in PBS. After rinsing wells with PBS four times, 40 pmol of PapD in 3% (w/v) BSA/PBS was added to each well. Plates were incubated for 1 h and then rinsed with PBS four times. PapD binding subsequently was detected by a standard colorimetric ELISA (Kuehn *et al.*, 1993; Xu *et al.*, 1995) using mouse α-PapDK, alkaline phosphatase-conjugated α-mouse IgG and nitrophenyl phosphate substrate.

Purification of fibrillae from PapA constructs

HB101 strains containing the PapA constructs were grown in Luria broth (pH 7.4) medium containing the appropriate antibiotics up to an optical density of 0.6 at 600 nm, prior to induction with 0.1 mM IPTG for 60 min. Cells subsequently were spun down and resuspended in 5 mM Tris and 75 mM NaCl (pH 8) and heated for 30 min at 65°C to extract surface tips and/or pili. Additional purification steps involved either magnesium-induced precipitation or Gal-α(1,4)-Gal affinity chromatography. Magnesium-induced precipitation of PapA-containing pili was carried out by adding NaCl to a final concentration of 250 mM and $MgCl_2$ to a final concentration of 100 mM. Affinity purification of PapG-containing whole pili and tip fibrillae was carried out by applying samples to a slurry of Gal-α(1,4)-Gal–Sepharose beads prepared as described previously (Hultgren *et al.*, 1989). After several washes, the bound structures were eluted with 50 mM ethyl-β galabioside.

Electron microscopy

Gal-α(1,4)-Gal affinity-purified pili were prepared for electron microscopy by adsorption to mica chips that were quick-frozen, then freeze-fractured and deep-etched before rotary replication with platinum as described previously (Heuser, 1989).

X-ray crystallography

PapD was prepared as previously described (Holmgren *et al.*, 1988). The peptide K(1′–19′) was prepared by F_{moc} solid-phase synthesis and purified by reversed-phase HPLC (Karlsson *et al.*, 1996). Crystals of the PapD–PapK-peptide complex were grown by vapor diffusion against 20% PEG 8000, 0.1 M MES pH 6.5. The crystallization drop contained equal volumes of reservoir and protein solution. The protein solution (15 mg/ml) contained a 1:1 molar ratio of PapD to peptide in 20 mM MES pH 6.5 with 1.0% β-octyl glucoside. The resulting crystals belong to space group, C2221 [thus differing from the PapD–PapG-peptide crystals which were C2 (Kuehn *et al.*, 1993)], with cell dimensions a = 57.2 Å, b = 153.8 Å, c = 135.9 Å and α = β = γ = 90°, two molecules in the asymmetric unit. The crystals diffract to 2.7 Å resolution on a lab X-ray source though only data to 2.8 Å resolution was used for structure determination.

The intensity data for the PapD–PapK-peptide crystals were collected on a R-AXIS II area-detector system at Symbicom AB, Uppsala. All data were obtained from a single crystal and processed initially with the DENZO software package (Otwinowski, 1993). Merging and scaling of the data were carried out using ROTAVATA and AGROVATA from the CCP4 package (CCP4, 1994). The final data set contained 16 071 independent reflections with an R_{sym} of 7.5% for data between 20.0 and 2.8 Å resolution.

The structure of the complex was solved by molecular replacement using the program XPLOR (Brünger, 1992). The search model used was the refined 2.0 Å resolution structure of PapD (Holmgren and Brändén, 1989). Using 8.0–4.0 Å resolution data, the self-rotation function again gave a clear non-crystallographic 2-fold axis. The top peaks in the translation functions also gave the correct solutions. After the translation functions, the R-factor was 36.7% for 8.0–4.0 Å resolution data. Subsequent rigid body refinement in which all four domains of the two PapD molecules in the asymmetric unit were allowed to refine independently resulted in an R-factor of 33.6% for the same data.

Examination of an $|F_o–F_c|$ electron density map at this stage using the graphics program O (Jones *et al.*, 1991) showed clear density corresponding to the K-peptide in the PapD cleft and running along the surface of the protein in an analogous fashion to that found in the PapD–G-peptide complex. The correct orientation of the peptide was determined easily from the electron density. Subsequent simulated annealing and atomic positional refinement was carried out with X-PLOR. Non-crystallographic restraints were applied throughout the refinement procedure. The model at the present level of refinement (which contains no water molecules and does not include the first five N-terminal amino acids of the peptide) has an R-factor of 19.2% and has r.m.s.ds from ideal geometry of 0.019 Å for bond lengths and 3.9° for bond angles.

Calculation of accessible solvent areas was performed using the algorithm of Lee and Richards (1971).

Assessment of chaperone–subunit complex formation

HB101 or KS474 strains containing PapD together with the appropriate *papA* or *papG* construct were grown in Luria broth (pH 7.4) medium containing the appropriate antibiotics up to an optical density of 0.6 at 600 nm, prior to induction with 0.5% arabinose and 1 mM IPTG for 90 min. After harvesting, periplasmic extracts were prepared as described previously (Slonim *et al.*, 1992). Pharmacia 3–9 isoelectric focusing gels were run according to the manufacturer and silver stained using the Phast system (Pharmacia).

Other methods

SDS–PAGE, isoelectric focusing and Western blot analysis were performed as previously described (Slonim *et al.*, 1992; Dodson *et al.*, 1993; Xu *et al.*, 1995).

Acknowledgements

This work was supported by National Institutes of Health grants R01AI29549 and R01DK51406.

References

Bacon,D.J. and Anderson,W.F. (1988) A fast algorithm for rendering space-filling molecular pictures. *J. Mol. Graph.*, **6**, 219–220.

Baga,M., Norgren,M. and Normark,S. (1987) Biogenesis of *E.coli* Pap pili: papH, a minor pilin subunit involved in cell anchoring and length modulation. *Cell*, **49**, 241–251.

Boyer,H.W. and Roulland-Dussoix,D. (1969) A complementation analysis of the restriction and modification of DNA in *Escherichia coli*. *J. Mol. Biol.*, **41**, 459–472.

Brünger,A.T. (1992) *X-PLOR Manual, Version 3.1*. Yale University Press, New Haven, CT.

Bullitt,E. and Makowski,L. (1993) Structural polymorphism of bacterial adhesion pili. *Nature*, **373**, 164–167.

Bullitt,E., Jones,C.H., Striker,R., Soto,G., Jacob-Dubuisson,F., Pinkner,J., Wick,M.J., Makowski,L. and Hultgren,S.J. (1996) Development of pilus organelle subassemblies *in vitro* depends on chaperone uncapping of a β zipper. *Proc. Natl Acad. Sci. USA*, **93**, 12890–12895.

CCP4 (1994) Collaborative computational project number 4. The CCP4 suite of programs for protein crystallography. *Acta Crystallogr.*, **D50**, 760–763.

DasGupta,U., Weston-Hafer,K. and Berg,D.E. (1987) Local DNA sequence control of deletion formation in *Escherichia coli* plasmid pBR322. *Genetics*, **115**, 41–49.

Derber,C.M. and Goto,N.K. (1996) Folding proteins into membranes. *Nature Struct. Biol.*, **3**, 815–818.

Dodson,K.W., Jacob-Dubuisson,F., Striker,R.T. and Hultgren,S.J. (1993) Outer-membrane PapC molecular usher discriminately recognizes periplasmic chaperone–pilus subunit complexes. *Proc. Natl Acad. Sci. USA*, **90**, 3670–3674.

Engelman,D.M. and Steitz,T.A. (1981) The spontaneous insertion of proteins into and across membranes: the helical hairpin hypothesis. *Cell*, **23**, 411–422.

Finkelstein,A.V. (1991) Rate of β-structure formation in polypeptides. *Proteins*, **9**, 23–27.

Gong,M. and Makowski,L. (1992) Helical structure of P pili from *Escherichia coli*. *J. Mol. Biol.*, **228**, 735–742.

Hamada,D., Segawa,S. and Goto,Y. (1996) Non-native α-helical intermediate in the refolding of β-lactoglobulin, a predominantly β-sheet protein. *Nature Struct. Biol.*, **3**, 868–873.

Heuser,J. (1989) Protocol for 3-D visualization of molecules on mica via the quick-freeze, deep-etch technique. *J. Electron Microsc. Tech.*, **13**, 244–263.

Holmgren,A. and Brändén,C.I. (1989) Crystal structure of chaperone protein PapD reveals an immunoglobulin fold. *Nature*, **342**, 248–251.

Holmgren,A., Brändén,C.I., Lindberg,F. and Tennent,J.M. (1988) Preliminary X-ray study of PapD crystals from uropathogenic *Escherichia coli*. *J. Mol. Biol.*, **203**, 279–280.

Holmgren,A., Kuehn,M.J., Brändén,C.I. and Hultgren,S.J. (1992) Conserved immunoglobulin-like features in a family of periplasmic pilus chaperones in bacteria. *EMBO J.*, **11**, 1617–1622.

Hultgren,S.J., Lindberg,F., Magnusson,G., Kihlberg,J., Tennent,J.M. and Normark,S. (1989) The PapG adhesin of uropathogenic *Escherichia coli* contains separate regions for receptor binding and for the incorporation into the pilus. *Proc. Natl Acad. Sci. USA*, **86**, 4357–4361.

Hultgren,S.J., Jones,C.H. and Normark,S. (1996) Bacterial adhesins and their assembly. In Neidhardt,F.C. (ed.), *Escherichia coli and Salmonella: Cellular and Molecular Biology*. ASM Press, Washington DC, pp. 2730–2756.

Hung,D.L., Knight,S.D., Woods,R.M., Pinkner,J.S. and Hultgren,S.J. (1996) Molecular basis of two subfamilies of immunoglobulin-like chaperones. *EMBO J.*, **15**, 3792–3805.

Jacob-Dubuisson,F., Heuser,J., Dodson,K., Normark,S. and Hultgren,S. (1993) Initiation of assembly and association of the structural elements of a bacterial pilus depend on two specialized tip proteins. *EMBO J.*, **12**, 837–847.

Jacob-Dubuisson,F., Striker,R. and Hultgren,S.J. (1994a) Chaperone-assisted self-assembly of pili independent of cellular energy. *J. Biol. Chem.*, **269**, 12447–12455.

Jacob-Dubuisson,F., Pinkner,J., Xu,Z., Striker,R., Padmanhaban,A. and Hultgren,S.J. (1994b) PapD chaperone function in pilus biogenesis depends on oxidant and chaperone-like activities of DsbA. *Proc. Natl Acad. Sci. USA*, **91**, 11552–11556.

Jones,C.H., Dodson,K. and Hultgren S.J. (1996) Structure, function and assembly of adhesive P pili. In Mobley,H.L.T. and Warren,J.W. (eds), *Urinary Tract Infections: Molecular Pathogenesis and Clinical Management*. ASM Press, Washington DC, pp. 175–219.

Jones,C.H., Danese,P.N., Pinkner,J.S., Silhavy,T.J. and Hultgren,S.J. (1997) The chaperone-assisted membrane release and folding pathway is sensed by two signal transduction systems. *EMBO J.*, **16**, 6394–6406.

Jones,S. and Thornton,J.M. (1995) Protein–protein interactions: a review of protein dimer structures. *Prog. Biophys. Mol. Biol.*, **63**, 31–65.

Jones,S. and Thornton,J.M. (1996) Principles of protein–protein interactions. *Proc. Natl Acad. Sci. USA*, **93**, 13–20.

Jones,T.A., Zou,J.Y., Cowan,S.W. and Kjelgaard,M. (1991) Improved methods for building protein models in electron density maps and the location of errors in these models. *Acta Crystallogr.*, **A47**, 110–119.

Karlsson,K.F., Walse,B., Drakenberg,T. and Kihlberg,J. (1996) Synthesis and conformational studies of peptides from *E.coli* pilus proteins recognized by the chaperone PapD. *Lett. Pept. Sci.*, **3**, 143–156.

Kraulis,P.J. (1991) MOLSCRIPT: a program to produce both detailed and schematic plots of protein structures. *J. Appl. Crystallogr.*, **24**, 946–950.

Kuehn,M.J., Heuser,J., Normark,S. and Hultgren,S.J. (1992) P pili in uropathogenic *E.coli* are composite fibres with distinct fibrillar adhesive tips. *Nature*, **356**, 252–255.

Kuehn,M.J., Ogg,D.J., Kihlberg,J., Slonim,L.N., Flemmer,K., Bergfors,T. and Hultgren,S.J. (1993) Structural basis of pilus subunit recognition by the PapD chaperone. *Science*, **262**, 1234–1241.

Lech,K. and Brent,R. (1987) Selected topics from classical bacterial genetics. In Ausubel,F.M., Brent,R., Kingston,R.E., Moore,D.D., Seidman J.G., Smith,J.A. and Struhl,K. (eds), *Current Protocols in Molecular Biology*. Greene Publishing Associates and Wiley Interscience, New York, NY, unit 1.4.

Lee,B. and Richards,F.M. (1971) The interpretation of protein structures: estimation of static accessibility. *J. Mol. Biol.*, **55**, 379–400.

Merritt,E.A. and Murphy,M.E.P. (1994) Raster3D version 2.0: a program for photorealistic molecular graphics. *Acta Crystallogr.*, **D50**, 869–873.

Minor,D.L.,Jr and Kim,P.S. (1994) Context is a major determinant of β-sheet propensity. *Nature*, **371**, 264–267.

Morrison,H.G. and Desrosiers,R.C. (1993) A PCR-based strategy for extensive mutagenesis of a target DNA sequence. *BioTechniques*, **14**, 454–457.

Normark,S., Båga,M., Göransson,M., Lindberg,F.P., Lund,B., Norgren,M. and Uhlin,B. (1986) Genetics and biogenesis of *Escherichia coli* adhesins. In Mirelman,D. (ed.), *Microbial Lectins and Agglutinins*. John Wiley and Sons, New York, NY, pp. 113–143.

Oliver,D.B. (1996) Periplasm. In Neidhardt,F.C. (ed.), *Escherichia coli and Salmonella: Cellular and Molecular Biology*. ASM Press, Washington DC, pp. 88–103.

Otwinowski,Z. (1993) Data collection and processing. In *Proceedings of CCP4 Study Weekend 29–30 January 1991*. SERC Daresbury Laboratory, UK.

Saulino,E.T., Thanassi,D.G., Pinkner,J. and Hultgren,S.J. (1998) Ramifications of kinetic partitioning on usher-mediated pilus biogenesis. *EMBO J.*, **17**, 2177–2185.

Slonim,L.N., Pinkner,J.S., Brändén,C. and Hultgren,S.J. (1992) Interactive surface in the PapD chaperone cleft is conserved in pilus chaperone superfamily and essential in subunit recognition and assembly. *EMBO J.*, **11**, 4747–4756.

Stites,W.E. (1997) Protein–protein interactions: interface structure, binding thermodynamics and mutational analysis. *Chem. Rev.*, **97**, 1233–1250.

Strauch,K.L., Johnson,K. and Beckwith,J. (1989) Characterization of *degP*, a gene required for proteolysis in the cell envelope of *Escherichia coli* at high temperature. *J. Bacteriol.*, **171**, 2689–2696.

Striker,R., Jacob-Dubuisson,F., Frieden,C. and Hultgren,S.J. (1994) Stable fiber-forming and nonfiber-forming chaperone–subunit complexes in pilus biogenesis. *J. Biol. Chem.*, **269**, 12233–12239.

Thanassi,D.G., Saulino,E.T., Lombardo,M.J., Roth,R., Heuser,J. and Hultgren,S.J. (1998) The PapC usher forms an oligomeric channel: implications for pilus biogenesis across the outer membrane. *Proc. Natl Acad. Sci. USA*, **95**, 3146–3151.

Wimley,W.C. and White,S.H. (1996) Experimentally determined hydrophobicity scale for proteins at membrane interfaces. *Nature Struct. Biol.*, **3**, 842–848.

Xu,Z., Jones,C.H., Haslem,D., Pinkner,J.S., Dodson,K., Kihlberg,J. and Hultgren,S.J. (1995) Molecular dissection of PapD interaction with PapG reveals two chaperone-binding sites. *Mol. Microbiol.*, **16**, 1011–1020.

Received June 11, 1998; revised September 1, 1998; acccepted September 8, 1998